

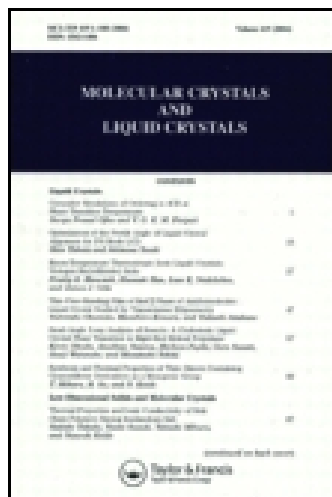
This article was downloaded by: [University of South Florida]

On: 31 October 2014, At: 08:22

Publisher: Taylor & Francis

Informa Ltd Registered in England and Wales Registered Number: 1072954

Registered office: Mortimer House, 37-41 Mortimer Street, London W1T 3JH, UK



Molecular Crystals and Liquid Crystals

Publication details, including instructions for authors and subscription information:

<http://www.tandfonline.com/loi/gmcl20>

Chirality-Induced Liquid Crystalline Properties of Seven-Ring Trimeric Mesogens Incorporating Dual Chiral Centers

Guan-Yeow Yeap^a, Tiang-Chuan Hng^a, Wan Ahmad Kamil Mahmood^a, Ewa Gorecka^b, Daisuke Takeuchi^c & Kohtaro Osakada^c

^a Liquid Crystal Research Laboratory, School of Chemical Sciences, Universiti Sains Malaysia, Penang, Malaysia

^b Department of Chemistry, Warsaw University, Warsaw, Poland

^c Chemical Resources Laboratory, Tokyo Institute of Technology, Midori-ku, Yokohama, Japan

Published online: 03 Aug 2009.

To cite this article: Guan-Yeow Yeap, Tiang-Chuan Hng, Wan Ahmad Kamil Mahmood, Ewa Gorecka, Daisuke Takeuchi & Kohtaro Osakada (2009) Chirality-Induced Liquid Crystalline Properties of Seven-Ring Trimeric Mesogens Incorporating Dual Chiral Centers, *Molecular Crystals and Liquid Crystals*, 506:1, 109-133, DOI: [10.1080/15421400902841353](https://doi.org/10.1080/15421400902841353)

To link to this article: <http://dx.doi.org/10.1080/15421400902841353>

PLEASE SCROLL DOWN FOR ARTICLE

Taylor & Francis makes every effort to ensure the accuracy of all the information (the "Content") contained in the publications on our platform. However, Taylor & Francis, our agents, and our licensors make no representations or warranties whatsoever as to the accuracy, completeness, or suitability for any purpose of the Content. Any opinions and views expressed in this publication are the opinions and views of the authors, and are not the views of or endorsed by Taylor & Francis. The accuracy of the Content should not be relied upon and should be independently verified with primary sources of information. Taylor and Francis shall not be liable for any losses, actions, claims, proceedings, demands, costs, expenses, damages, and other liabilities whatsoever or howsoever caused arising directly or indirectly in connection with, in relation to or arising out of the use of the Content.

This article may be used for research, teaching, and private study purposes. Any substantial or systematic reproduction, redistribution, reselling, loan, sub-licensing, systematic supply, or distribution in any form to anyone is expressly forbidden. Terms & Conditions of access and use can be found at <http://www.tandfonline.com/page/terms-and-conditions>

Chirality-Induced Liquid Crystalline Properties of Seven-Ring Trimeric Mesogens Incorporating Dual Chiral Centers

Guan-Yeow Yeap¹, Tiang-Chuan Hng¹, Wan Ahmad Kamil Mahmood¹, Ewa Gorecka², Daisuke Takeuchi³, and Kohtaro Osakada³

¹Liquid Crystal Research Laboratory, School of Chemical Sciences, Universiti Sains Malaysia, Penang, Malaysia

²Department of Chemistry, Warsaw University, Warsaw, Poland

³Chemical Resources Laboratory, Tokyo Institute of Technology, Midori-ku, Yokohama, Japan

Two series of novel trimers with benzylidene-1,4-phenylenediamine core units attached by two (S)-2-methylbutyl 4-(4'-phenyl)benzoate moieties via methylene groups at terminal ends have been synthesized and characterized. In each series, the title compounds differ from each other in term of spacers $-OC_nH_{2n}O-$ wherein n ranges from 5 to 12. The difference of the second series from their analogues in the first series is due to the presence of two OCH_3 groups residing at the meta position in the benzylidene-1,4-phenylenediamine mesogenic core. The trimers without lateral OCH_3 groups exhibit the SmC^ and SmA phases in addition to the N^* phase suggesting the possession of high molecular shape anisotropy. The higher-order tilted smectic phases and the blue phase are also observed for the members with odd n numbers in the first series. In the second series, however, the smectogenic characteristics are absent. Whilst the even-parity trimers are nematogenic, the trimers with odd spacers are not mesogenic. The trimers without lateral OCH_3 groups in the first series also exhibit higher mesophase thermal stability in comparison with their analogues in the second series.*

1. INTRODUCTION

In contrast with conventional polymers, semiflexible main chain liquid crystal polymers are composed of alternating rigid mesogenic fragments and flexible groups such as the alkyl chains [1]. Liquid crystal dimers

Address correspondence to Guan-Yeow Yeap, Liquid Crystal Research Laboratory, School of Chemical Sciences, Universiti Sains Malaysia, 11800 Minden, Penang, Malaysia. E-mail: gyyeap_liqcryst_usm@yahoo.com

are often used as model compounds reflecting these polymers as their transitional properties in many ways possess similarities to those of the polymeric system [2]. One of these properties is the significant odd–even effect exhibited by the clearing temperatures of the dimers. However, the liquid crystalline behavior of these dimers is different in comparison with the conventional liquid crystals which contain only one mesogenic fragment and two flexible terminal groups.

The unique characteristics of liquid crystal dimers have then prompted many researchers to study the liquid crystal oligomers [3–5]. One of the liquid crystal oligomers is called *trimer* which consists of three mesogenic fragments connected by two methylene spacers [2]. Previous investigations showed that the physical properties of the trimers were different from those of the dimers and monomers wherein the magnitude of the alternation exhibited by T_{NI} upon changing the number of carbon atoms in the spacers linking the mesogenic cores of the 4,4'-bis[ω -(4-cyanobiphenyl-4'-yloxy)alkoxy] biphenyls was slightly greater than that exhibited by the dimers [6].

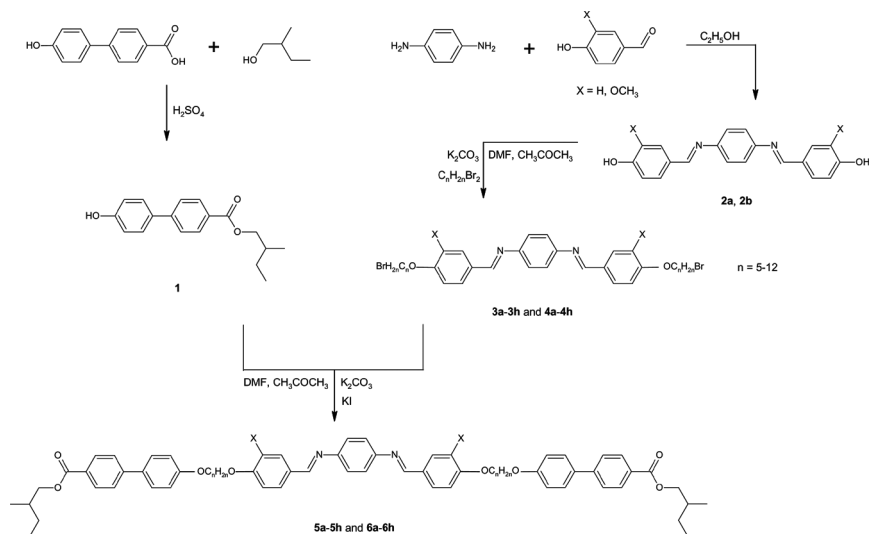
As far as liquid crystals are concerned, chirality and chirality-induced properties are amongst the key features towards the development of high-tech materials for display and thermochromic devices, electro-optics, and many other applications. In addition to the wide application of chiral liquid crystal materials, researchers are also interested in chirally induced phenomena as appearance of twist-grain boundary (TGB) phases, polar smectic phases, and various blue phases [7–11]. However, until today only a few chiral trimeric liquid crystals have been reported [12,13].

In this report we present a comprehensive study on two series of novel symmetric trimers with two chiral centers. The sixteen title compounds are synthesized in which the benzylidene-1,4-phenylenediamine serves as the rigid core joining up (*S*)-2-methylbutyl-4-(4'-phenyl)benzoate moiety via respective methylene group. In our present study, the spacers with odd and even-parity ranging from C_5H_{10} to $C_{12}H_{24}$ are introduced into the trimeric system. Among these trimers, the thermal stability between the members with and without the two lateral methoxy (OCH_3) groups in the central core as well as the influence of these OCH_3 groups on the chiral mesomorphic properties will be documented.

2. EXPERIMENTAL

2.1. Synthesis

The liquid crystal trimers were synthesized according to the synthetic routes as given in scheme 1. Compound **1** is a product derived from the



SCHEME 1 The synthetic routes toward formation of liquid crystal trimers **5a-5h** and **6a-6h**.

Fischer acid-catalyzed esterification in the presence of concentrated sulphuric acid. Compounds **2a** and **2b** were synthesized via condensation reaction from *p*-phenylenediamine with *p*-hydroxybenzaldehyde and vanillin, respectively [14]. In order to obtain compounds **3a-3h** and **4a-4h**, the intermediary **2a** and **2b** were alkylated with a series of α,ω -dibromoalkanes via Williamson synthesis in the presence of potassium carbonate anhydrous. The title compounds **5a-5h** (first series) and **6a-6h** (second series) are the products obtained from the alkylation between compound **1** and **3a-3h** and **4a-4h**, respectively, in which the potassium carbonate anhydrous and potassium iodide were used as catalysts. These compounds with respective lateral substituents (H or OCH_3) and spacers (C_5H_{10} to $C_{12}H_{24}$) are tabulated in Table 1.

2.1.1. Synthesis of Compound 1

4-(4-Hydroxyphenyl)benzoic acid (1.50 g, 7.0 mmole) was added to 25 mL (*S*)-2-methyl-1-butanol in a round-bottom flask and refluxed at $90^\circ C$ for 24 h. A few drops of concentrated H_2SO_4 were added dropwise to the mixture. The resulting solution was left to evaporate off at room temperature and the crude product was then recrystallized thrice from hexane and chloroform mixture to yield the white intermediate. Yield 70%. Elemental analysis (%): found, C 76.04, H 7.11;

TABLE 1 List of Intermediary and Title Compounds with Respective Lateral Substituents, X and Spacers, C_nH_{2n} in the First and Second Series

Compound	Lateral substituent, X	Spacer (-C _n H _{2n} -)
3a	H	C ₅ H ₁₀
3b	H	C ₆ H ₁₂
3c	H	C ₇ H ₁₄
3d	H	C ₈ H ₁₆
3e	H	C ₉ H ₁₈
3f	H	C ₁₀ H ₂₀
3g	H	C ₁₁ H ₂₂
3h	H	C ₁₂ H ₂₄
4a	OCH ₃	C ₅ H ₁₀
4b	OCH ₃	C ₆ H ₁₂
4c	OCH ₃	C ₇ H ₁₄
4d	OCH ₃	C ₈ H ₁₆
4e	OCH ₃	C ₉ H ₁₈
4f	OCH ₃	C ₁₀ H ₂₀
4g	OCH ₃	C ₁₁ H ₂₂
4h	OCH ₃	C ₁₂ H ₂₄
5a	H	C ₅ H ₁₀
5b	H	C ₆ H ₁₂
5c	H	C ₇ H ₁₄
5d	H	C ₈ H ₁₆
5e	H	C ₉ H ₁₈
5f	H	C ₁₀ H ₂₀
5g	H	C ₁₁ H ₂₂
5h	H	C ₁₂ H ₂₄
6a	OCH ₃	C ₅ H ₁₀
6b	OCH ₃	C ₆ H ₁₂
6c	OCH ₃	C ₇ H ₁₄
6d	OCH ₃	C ₈ H ₁₆
6e	OCH ₃	C ₉ H ₁₈
6f	OCH ₃	C ₁₀ H ₂₀
6g	OCH ₃	C ₁₁ H ₂₂
6h	OCH ₃	C ₁₂ H ₂₄

calculated (C₁₈H₂₀O₃), C 76.03, H 7.09. IR (KBr) ν /cm⁻¹, 3409 (OH), 2967–2878 (C-H alkyl), 1683 (C=O ester). ¹H-NMR (CDCl₃) δ /ppm, 0.97 (t, 3H, CH₃), 1.06 (d, 3H, CH₃), 1.34 (m, 1H, CH₂), 1.57 (m, 1H, CH₂), 1.91 (m, 1H, CH), 4.16–4.28 (2dd, 2H, OCH₂), 6.98 (d, 2H, Ar), 7.54 (d, 2H, Ar), 7.65 (d, 2H, Ar), 8.10 (d, 2H, Ar).

2.1.2. Synthesis of Compound 2a

In a round-bottom flask, 4-hydroxybenzaldehyde (2.55 g, 20.9 mmole) was dissolved in 70 mL absolute ethanol and heated to 40°C. A hot ethanolic solution of *p*-phenylenediamine (1.03 g, 9.5 mmole) was then

added dropwise, and the mixture was refluxed at 60°C for 24 h. The resulting solution was then left to evaporate at room temperature. The precipitate was finally purified with ethanol twice to give the pure yellow intermediary compound **2a**. Yield 85%. Elemental analysis (%): found, C 75.96, H 5.11, N 8.86; calculated (C₂₀H₁₆N₂O₂), C 75.93, H 5.10, N 8.86. IR (KBr) ν/cm^{-1} , 3274 (OH), 1618–1590 (C=N).

2.1.3. Synthesis of Compound 2b

Yield 80%. Elemental analysis (%): found, C 70.22, H 5.38, N 7.45; calculated (C₂₂H₂₀N₂O₄), C 70.20, H 5.36, N 7.44. IR (KBr) ν/cm^{-1} , 3385 (OH), 1621–1599 (C=N), 1285 (Ar-O-CH₃).

2.1.4. Synthesis of Compound 3a

In a round-bottom flask, compound **2a** (0.32 g, 1.0 mmole) was dissolved in minimal N,N-dimethylformamide solution prior to the addition of potassium carbonate anhydrous (0.69 g, 5.0 mmole). A solution of 1,5-dibromopentane (2.30 g, 10.0 mmole) in 50 mL acetone was then added dropwise to the mixture and subsequently refluxed for 18 h. The resulting mixture was left to evaporate at room temperature prior to the addition of water. The precipitate was then filtered off, dried and recrystallized from hexane and chloroform mixture to yield the pure yellow powder. Yield 60%. Elemental analysis (%): found, C 58.67, H 5.60, N 4.57; calculated (C₃₀H₃₄Br₂N₂O₂), C 58.65, H 5.58, N 4.56. IR (KBr) ν/cm^{-1} , 2949–2864 (C-H alkyl), 1617–1596 (C=N), 1247 (O-CH₂). ¹H-NMR (CDCl₃) δ/ppm , 1.66–2.02 (m, 12H, CH₂), 3.48 (t, 4H, CH₂Br), 4.07 (t, 4H, OCH₂), 7.01 (d, 4H, Ar), 7.27 (s, 4H, Ar), 7.86 (d, 4H, Ar), 8.46 (s, 2H, CH=N).

Compounds **3b–3h** and **4a–4h** were synthesized via similar method as described for compound **3a**. The analytical data for these compounds are shown in Sections 2.1.5–2.1.19.

2.1.5. Synthesis of Compound 3b

Yield 71%. Elemental analysis (%): found, C 59.84, H 5.99, N 4.35; calculated (C₃₂H₃₈Br₂N₂O₂), C 59.82, H 5.96, N 4.36. IR (KBr) ν/cm^{-1} , 2936–2857 (C-H alkyl), 1606 (C=N), 1249 (O-CH₂). ¹H-NMR (CDCl₃) δ/ppm , 1.55–1.96 (m, 16H, CH₂), 3.45 (t, 4H, CH₂Br), 4.08 (t, 4H, OCH₂), 7.01 (d, 4H, Ar), 7.28 (s, 4H, Ar), 7.88 (d, 4H, Ar), 8.46 (s, 2H, CH=N).

2.1.6. Synthesis of Compound 3c

Yield 58%. Elemental analysis (%): found, C 60.93, H 6.32, N 4.17; calculated (C₃₄H₄₂Br₂N₂O₂), C 60.90, H 6.31, N 4.18. IR (KBr) ν/cm^{-1} ,

2938–2852 (C-H alkyl), 1616–1597 (C=N), 1251 (O-CH₂). ¹H-NMR (CDCl₃) δ/ppm, 1.41–1.94 (m, 20H, CH₂), 3.45 (t, 4H, CH₂Br), 4.05 (t, 4H, OCH₂), 7.01 (d, 4H, Ar), 7.28 (s, 4H, Ar), 7.86 (d, 4H, Ar), 8.46 (s, 2H, CH=N).

2.1.7. Synthesis of Compound 3d

Yield 75%. Elemental analysis (%): found, C 61.92, H 6.66, N 3.99; calculated (C₃₆H₄₆Br₂N₂O₂), C 61.90, H 6.64, N 4.01. IR (KBr) ν/cm⁻¹, 2936–2856 (C-H alkyl), 1605 (C=N), 1250 (O-CH₂). ¹H-NMR (CDCl₃) δ/ppm, 1.39–1.91 (m, 24H, CH₂), 3.44 (t, 4H, CH₂Br), 4.05 (t, 4H, OCH₂), 7.01 (d, 4H, Ar), 7.28 (s, 4H, Ar), 7.86 (d, 4H, Ar), 8.46 (s, 2H, CH=N).

2.1.8. Synthesis of Compound 3e

Yield 57%. Elemental analysis (%): found, C 62.82, H 6.97, N 3.85; calculated (C₃₈H₅₀Br₂N₂O₂), C 62.81, H 6.94, N 3.86. IR (KBr) ν/cm⁻¹, 2918–2850 (C-H alkyl), 1603 (C=N), 1248 (O-CH₂). ¹H-NMR (CDCl₃) δ/ppm, 1.37–1.92 (m, 28H, CH₂), 3.44 (t, 4H, CH₂Br), 4.05 (t, 4H, OCH₂), 7.01 (d, 4H, Ar), 7.28 (s, 4H, Ar), 7.85 (d, 4H, Ar), 8.46 (s, 2H, CH=N).

2.1.9. Synthesis of Compound 3f

Yield 68%. Elemental analysis (%): found, C 63.67, H 7.23, N 3.72; calculated (C₄₀H₅₄Br₂N₂O₂), C 63.66, H 7.21, N 3.71. IR (KBr) ν/cm⁻¹, 2936–2850 (C-H alkyl), 1606 (C=N), 1248 (O-CH₂). ¹H-NMR (CDCl₃) δ/ppm, 1.37–1.93 (m, 32H, CH₂), 3.42 (t, 4H, CH₂Br), 4.07 (t, 4H, OCH₂), 7.01 (d, 4H, Ar), 7.28 (s, 4H, Ar), 7.88 (d, 4H, Ar), 8.46 (s, 2H, CH=N).

2.1.10. Synthesis of Compound 3g

Yield 52%. Elemental analysis (%): found, C 64.47, H 7.49, N 3.60; calculated (C₄₂H₅₈Br₂N₂O₂), C 64.45, H 7.47, N 3.58. IR (KBr) ν/cm⁻¹, 2919–2850 (C-H alkyl), 1602 (C=N), 1250 (O-CH₂). ¹H-NMR (CDCl₃) δ/ppm, 1.33–1.91 (m, 36H, CH₂), 3.44 (t, 4H, CH₂Br), 4.05 (t, 4H, OCH₂), 7.01 (d, 4H, Ar), 7.28 (s, 4H, Ar), 7.86 (d, 4H, Ar), 8.46 (s, 2H, CH=N).

2.1.11. Synthesis of Compound 3h

The synthetic route is similar to that described for **3a**. But, upon completion of reflux, the excess 1,12-dibromododecane was first removed with acetone and the desired precipitate was subsequently recrystallized from hexane and chloroform mixture. Yield 60%.

Elemental analysis (%): found, C 65.21, H 7.72, N 3.46; calculated ($C_{44}H_{62}Br_2N_2O_2$), C 65.18, H 7.71, N 3.46. IR (KBr) ν/cm^{-1} , 2935–2849 (C-H alkyl), 1606 (C=N), 1252 (O-CH₂). ¹H-NMR (CDCl₃) δ/ppm , 1.31–1.92 (m, 40H, CH₂), 3.43 (t, 4H, CH₂Br), 4.06 (t, 4H, OCH₂), 7.01 (d, 4H, Ar), 7.28 (s, 4H, Ar), 7.87 (d, 4H, Ar), 8.45 (s, 2H, CH=N).

2.1.12. Synthesis of Compound 4a

Yield 44%. Elemental analysis (%): found, C 57.00, H 5.69, N 4.17; calculated ($C_{32}H_{38}Br_2N_2O_4$), C 56.99, H 5.68, N 4.15. IR (KBr) ν/cm^{-1} , 2938–2866 (C-H alkyl), 1618–1595 (C=N), 1268 (O-CH₂). ¹H-NMR (CDCl₃) δ/ppm , 1.64–1.99 (m, 12H, CH₂), 3.48 (t, 4H, CH₂Br), 4.00 (s, 6H, OCH₃), 4.12 (t, 4H, OCH₂), 6.96 (d, 2H, Ar), 7.28 (s, 4H, Ar), 7.31 (dd, 2H, Ar), 7.64 (s, 2H, Ar), 8.44 (s, 2H, CH=N).

2.1.13. Synthesis of Compound 4b

Yield 65%. Elemental analysis (%): found, C 58.15, H 6.05, N 4.00; calculated ($C_{34}H_{42}Br_2N_2O_4$), C 58.13, H 6.03, N 3.99. IR (KBr) ν/cm^{-1} , 2935–2860 (C-H alkyl), 1619–1595 (C=N), 1270 (O-CH₂). ¹H-NMR (CDCl₃) δ/ppm , 1.55–1.94 (m, 16H, CH₂), 3.44 (t, 4H, CH₂Br), 4.00 (s, 6H, OCH₃), 4.12 (t, 4H, OCH₂), 6.97 (d, 2H, Ar), 7.28 (s, 4H, Ar), 7.33 (dd, 2H, Ar), 7.65 (s, 2H, Ar), 8.44 (s, 2H, CH=N).

2.1.14. Synthesis of Compound 4c

Yield 62%. Elemental analysis (%): found, C 59.22, H 6.36, N 3.83; calculated ($C_{36}H_{46}Br_2N_2O_4$), C 59.19, H 6.35, N 3.83. IR (KBr) ν/cm^{-1} , 2936–2857 (C-H alkyl), 1618–1595 (C=N), 1268 (O-CH₂). ¹H-NMR (CDCl₃) δ/ppm , 1.41–1.94 (m, 20H, CH₂), 3.44 (t, 4H, CH₂Br), 4.00 (s, 6H, OCH₃), 4.11 (t, 4H, OCH₂), 6.96 (d, 2H, Ar), 7.28 (s, 4H, Ar), 7.33 (dd, 2H, Ar), 7.65 (s, 2H, Ar), 8.44 (s, 2H, CH=N).

2.1.15. Synthesis of Compound 4d

Yield 70%. Elemental analysis (%): found, C 60.17, H 6.66, N 3.71; calculated ($C_{38}H_{50}Br_2N_2O_4$), C 60.16, H 6.64, N 3.69. IR (KBr) ν/cm^{-1} , 2937–2856 (C-H alkyl), 1617–1595 (C=N), 1269 (O-CH₂). ¹H-NMR (CDCl₃) δ/ppm , 1.38–1.93 (m, 24H, CH₂), 3.44 (t, 4H, CH₂Br), 4.00 (s, 6H, OCH₃), 4.11 (t, 4H, OCH₂), 6.96 (d, 2H, Ar), 7.28 (s, 4H, Ar), 7.33 (dd, 2H, Ar), 7.64 (s, 2H, Ar), 8.44 (s, 2H, CH=N).

2.1.16. Synthesis of Compound 4e

Yield 70%. Elemental analysis (%): found, C 61.08, H 6.94, N 3.55; calculated ($C_{40}H_{54}Br_2N_2O_4$), C 61.07, H 6.92, N 3.56. IR (KBr) ν/cm^{-1} , 2936–2854 (C-H alkyl), 1618–1596 (C=N), 1268 (O-CH₂).

$^1\text{H-NMR}$ (CDCl_3) δ/ppm , 1.36–1.92 (m, 28H, CH_2), 3.43 (t, 4H, CH_2Br), 4.00 (s, 6H, OCH_3), 4.10 (t, 4H, OCH_2), 6.96 (d, 2H, Ar), 7.28 (s, 4H, Ar), 7.31 (dd, 2H, Ar), 7.64 (s, 2H, Ar), 8.44 (s, 2H, $\text{CH}=\text{N}$).

2.1.17. Synthesis of Compound 4f

Yield 71%. Elemental analysis (%): found, C 61.94, H 7.19, N 3.43; calculated ($\text{C}_{42}\text{H}_{58}\text{Br}_2\text{N}_2\text{O}_4$), C 61.92, H 7.18, N 3.44. IR (KBr) ν/cm^{-1} , 2922–2854 (C-H alkyl), 1624–1597 (C=N), 1266 (O- CH_2). $^1\text{H-NMR}$ (CDCl_3) δ/ppm , 1.34–1.93 (m, 32H, CH_2), 3.43 (t, 4H, CH_2Br), 4.00 (s, 6H, OCH_3), 4.11 (t, 4H, OCH_2), 6.97 (d, 2H, Ar), 7.28 (s, 4H, Ar), 7.34 (dd, 2H, Ar), 7.64 (s, 2H, Ar), 8.44 (s, 2H, $\text{CH}=\text{N}$).

2.1.18. Synthesis of Compound 4g

Yield 73%. Elemental analysis (%): found, C 62.72, H 7.45, N 3.33; calculated ($\text{C}_{44}\text{H}_{62}\text{Br}_2\text{N}_2\text{O}_4$), C 62.71, H 7.42, N 3.32. IR (KBr) ν/cm^{-1} , 2925–2853 (C-H alkyl), 1619–1596 (C=N), 1269 (O- CH_2). $^1\text{H-NMR}$ (CDCl_3) δ/ppm , 1.30–1.92 (m, 36H, CH_2), 3.41 (t, 4H, CH_2Br), 4.01 (s, 6H, OCH_3), 4.11 (t, 4H, OCH_2), 6.97 (d, 2H, Ar), 7.28 (s, 4H, Ar), 7.33 (dd, 2H, Ar), 7.63 (s, 2H, Ar), 8.43 (s, 2H, $\text{CH}=\text{N}$).

2.1.19. Synthesis of Compound 4h

Upon completion of reflux, the excess 1,12-dibromododecane was first removed with acetone and the desired precipitate was subsequently recrystallized from hexane and chloroform mixture. Yield 58%. Elemental analysis (%): found, C 63.45, H 7.67, N 3.23; calculated ($\text{C}_{46}\text{H}_{66}\text{Br}_2\text{N}_2\text{O}_4$), C 63.44, H 7.64, N 3.22. IR (KBr) ν/cm^{-1} , 2928–2854 (C-H alkyl), 1623–1597 (C=N), 1267 (O- CH_2). $^1\text{H-NMR}$ (CDCl_3) δ/ppm , 1.31–1.93 (m, 40H, CH_2), 3.43 (t, 4H, CH_2Br), 4.00 (s, 6H, OCH_3), 4.11 (t, 4H, OCH_2), 6.96 (d, 2H, Ar), 7.28 (s, 4H, Ar), 7.32 (dd, 2H, Ar), 7.64 (s, 2H, Ar), 8.44 (s, 2H, $\text{CH}=\text{N}$).

2.1.20. Synthesis of Compound 5a

In a round-bottom flask, a mixture of compound **1** (0.28 g, 1.0 mmole), potassium carbonate anhydrous (0.28 g, 2.0 mmole) and catalytic amount of potassium iodide was heated with stirring in 50 mL acetone. Compound **3a** (0.25 g, 0.4 mmole) was dissolved in minimal N,N-dimethylformamide and subsequently added dropwise to the mixture. The overall mixture was heated under reflux for 18 h. The acetone was removed via evaporation at room temperature, and both potassium carbonate anhydrous and potassium iodide were removed with the addition of water. The excess compound **1** was removed using absolute ethanol and the desired product was finally recrystallized from ethyl acetate. Yield 50%. Elemental analysis (%): found, C

77.64, H 7.12, N 2.75; calculated ($C_{66}H_{72}N_2O_8$), C 77.62, H 7.11, N 2.74. IR (KBr) ν/cm^{-1} , 2949–2867 (C–H alkyl), 1711 (C=O ester), 1606 (C=N), 1251 (O–CH₂). ¹H-NMR (CDCl₃) δ/ppm , 0.99 (t, 6H, CH₃), 1.06 (d, 6H, CH₃), 1.34 (m, 2H, CH₂), 1.57–1.94 (m, 16H, CH and CH₂), 4.07–4.24 (2t and 2dd, 12H, OCH₂), 7.03 (2d, 8H, Ar), 7.28 (s, 4H, Ar), 7.58 (d, 4H, Ar), 7.66 (d, 4H, Ar), 7.86 (d, 4H, Ar), 8.10 (d, 4H, Ar), 8.46 (s, 2H, CH=N).

Compounds **5b–5h** and **6a–6h** were synthesized via similar steps as mentioned for compound **5a**. The analytical data for these compounds are listed in Sections 2.1.21–2.1.35.

2.1.21. Synthesis of Compound 5b

Yield 52%. Elemental analysis (%): found, C 77.85, H 7.31, N 2.68; calculated ($C_{68}H_{76}N_2O_8$), C 77.83, H 7.30, N 2.67. IR (KBr) ν/cm^{-1} , 2940–2875 (C–H alkyl), 1715 (C=O ester), 1604 (C=N), 1249 (O–CH₂). ¹H-NMR (CDCl₃) δ/ppm , 1.01 (t, 6H, CH₃), 1.07 (d, 6H, CH₃), 1.34 (m, 2H, CH₂), 1.57–1.91 (m, 20H, CH and CH₂), 4.06–4.26 (2t and 2dd, 12H, OCH₂), 7.02 (2d, 8H, Ar), 7.26 (s, 4H, Ar), 7.56 (d, 4H, Ar), 7.65 (d, 4H, Ar), 7.86 (d, 4H, Ar), 8.09 (d, 4H, Ar), 8.46 (s, 2H, CH=N).

2.1.22. Synthesis of Compound 5c

Yield 56%. Elemental analysis (%): found, C 78.04, H 7.50, N 2.62; calculated ($C_{70}H_{80}N_2O_8$), C 78.04, H 7.48, N 2.60. IR (KBr) ν/cm^{-1} , 2940–2868 (C–H alkyl), 1715 (C=O ester), 1604 (C=N), 1249 (O–CH₂). ¹H-NMR (CDCl₃) δ/ppm , 0.99 (t, 6H, CH₃), 1.06 (d, 6H, CH₃), 1.34 (m, 2H, CH₂), 1.54–1.91 (m, 24H, CH and CH₂), 4.03–4.22 (2t and 2dd, 12H, OCH₂), 7.02 (2d, 8H, Ar), 7.27 (s, 4H, Ar), 7.57 (d, 4H, Ar), 7.65 (d, 4H, Ar), 7.86 (d, 4H, Ar), 8.09 (d, 4H, Ar), 8.46 (s, 2H, CH=N).

2.1.23. Synthesis of Compound 5d

Yield 59%. Elemental analysis (%): found, C 78.24, H 7.69, N 2.55; calculated ($C_{72}H_{84}N_2O_8$), C 78.23, H 7.66, N 2.53. IR (KBr) ν/cm^{-1} , 2935–2856 (C–H alkyl), 1716 (C=O ester), 1605 (C=N), 1249 (O–CH₂). ¹H-NMR (CDCl₃) δ/ppm , 1.01 (t, 6H, CH₃), 1.07 (d, 6H, CH₃), 1.34 (m, 2H, CH₂), 1.57–1.92 (m, 28H, CH and CH₂), 4.04–4.29 (2t and 2dd, 12H, OCH₂), 7.02 (2d, 8H, Ar), 7.25 (s, 4H, Ar), 7.56 (d, 4H, Ar), 7.64 (d, 4H, Ar), 7.85 (d, 4H, Ar), 8.09 (d, 4H, Ar), 8.45 (s, 2H, CH=N).

2.1.24. Synthesis of Compound 5e

Yield 52%. Elemental analysis (%): found, C 78.42, H 7.85, N 2.49; calculated ($C_{74}H_{88}N_2O_8$), C 78.41, H 7.83, N 2.47. IR (KBr) ν/cm^{-1} ,

2937–2851 (C-H alkyl), 1706 (C=O ester), 1605 (C=N), 1249 (O-CH₂). ¹H-NMR (CDCl₃) δ/ppm, 0.99 (t, 6H, CH₃), 1.06 (d, 6H, CH₃), 1.34 (m, 2H, CH₂), 1.41–1.92 (m, 32H, CH and CH₂), 4.02–4.24 (2t and 2dd, 12H, OCH₂), 7.00 (2d, 8H, Ar), 7.27 (s, 4H, Ar), 7.57 (d, 4H, Ar), 7.63 (d, 4H, Ar), 7.85 (d, 4H, Ar), 8.10 (d, 4H, Ar), 8.45 (s, 2H, CH=N).

2.1.25. Synthesis of Compound 5f

Yield 50%. Elemental analysis (%): found, C 78.60, H 8.00, N 2.42; calculated (C₇₆H₉₂N₂O₈), C 78.58, H 7.98, N 2.41. IR (KBr) ν/cm⁻¹, 2936–2852 (C-H alkyl), 1715 (C=O ester), 1604 (C=N), 1250 (O-CH₂). ¹H-NMR (CDCl₃) δ/ppm, 1.00 (t, 6H, CH₃), 1.07 (d, 6H, CH₃), 1.34 (m, 2H, CH₂), 1.40–1.94 (m, 36H, CH and CH₂), 4.03–4.29 (2t and 2dd, 12H, OCH₂), 7.02 (2d, 8H, Ar), 7.28 (s, 4H, Ar), 7.56 (d, 4H, Ar), 7.64 (d, 4H, Ar), 7.85 (d, 4H, Ar), 8.08 (d, 4H, Ar), 8.45 (s, 2H, CH=N).

2.1.26. Synthesis of Compound 5g

Yield 58%. Elemental analysis (%): found, C 78.78, H 8.15, N 2.35; calculated (C₇₈H₉₆N₂O₈), C 78.75, H 8.13, N 2.35. IR (KBr) ν/cm⁻¹, 2937–2850 (C-H alkyl), 1708 (C=O ester), 1605 (C=N), 1248 (O-CH₂). ¹H-NMR (CDCl₃) δ/ppm, 0.99 (t, 6H, CH₃), 1.06 (d, 6H, CH₃), 1.34–1.91 (m, 42H, CH and CH₂), 4.03–4.26 (2t and 2dd, 12H, OCH₂), 7.01 (2d, 8H, Ar), 7.27 (s, 4H, Ar), 7.57 (d, 4H, Ar), 7.65 (d, 4H, Ar), 7.85 (d, 4H, Ar), 8.10 (d, 4H, Ar), 8.45 (s, 2H, CH=N).

2.1.27. Synthesis of Compound 5h

Yield 70%. Elemental analysis (%): found, C 78.94, H 8.30, N 2.29; calculated (C₈₀H₁₀₀N₂O₈), C 78.91, H 8.28, N 2.30. IR (KBr) ν/cm⁻¹, 2935–2850 (C-H alkyl), 1716 (C=O ester), 1605 (C=N), 1250 (O-CH₂). ¹H-NMR (CDCl₃) δ/ppm, 1.01 (t, 6H, CH₃), 1.07 (d, 6H, CH₃), 1.34–1.91 (m, 46H, CH and CH₂), 4.03–4.28 (2t and 2dd, 12H, OCH₂), 7.02 (2d, 8H, Ar), 7.25 (s, 4H, Ar), 7.56 (d, 4H, Ar), 7.64 (d, 4H, Ar), 7.85 (d, 4H, Ar), 8.08 (d, 4H, Ar), 8.45 (s, 2H, CH=N).

2.1.28. Synthesis of Compound 6a

Yield 60%. Elemental analysis (%): found, C 75.54, H 7.10, N 2.61; calculated (C₆₈H₇₆N₂O₁₀), C 75.53, H 7.08, N 2.59. IR (KBr) ν/cm⁻¹, 2951–2871 (C-H alkyl), 1711 (C=O ester), 1618–1603 (C=N), 1268 (O-CH₂). ¹H-NMR (CDCl₃) δ/ppm, 0.99 (t, 6H, CH₃), 1.06 (d, 6H, CH₃), 1.34 (m, 2H, CH₂), 1.57–2.01 (m, 16H, CH and CH₂), 4.00 (s, 6H, OCH₃), 4.06–4.24 (2t and 2dd, 12H, OCH₂), 6.97 (d, 2H, Ar), 7.02 (d, 4H, Ar), 7.28 (s, 4H, Ar), 7.31 (dd, 2H, Ar), 7.58 (d, 4H, Ar), 7.63 (s and d, 6H, Ar), 8.09 (d, 4H, Ar), 8.44 (s, 2H, CH=N).

2.1.29. Synthesis of Compound 6b

Yield 49%. Elemental analysis (%): found, C 75.79, H 7.29, N 2.51; calculated (C₇₀H₈₀N₂O₁₀), C 75.78, H 7.27, N 2.52. IR (KBr) ν/cm^{-1} , 2932–2854 (C–H alkyl), 1713 (C=O ester), 1620–1602 (C=N), 1268 (O–CH₂). ¹H-NMR (CDCl₃) δ/ppm , 0.99 (t, 6H, CH₃), 1.06 (d, 6H, CH₃), 1.34 (m, 2H, CH₂), 1.57–1.94 (m, 20H, CH and CH₂), 4.00 (s, 6H, OCH₃), 4.04–4.26 (2t and 2dd, 12H, OCH₂), 6.97 (d, 2H, Ar), 7.02 (d, 4H, Ar), 7.28 (s, 4H, Ar), 7.31 (dd, 2H, Ar), 7.57 (d, 4H, Ar), 7.63 (2d, 6H, Ar), 8.09 (d, 4H, Ar), 8.44 (s, 2H, CH=N).

2.1.30. Synthesis of Compound 6c

Yield 64%. Elemental analysis (%): found, C 76.04, H 7.45, N 2.45; calculated (C₇₂H₈₄N₂O₁₀), C 76.03, H 7.44, N 2.46. IR (KBr) ν/cm^{-1} , 2935–2857 (C–H alkyl), 1712 (C=O ester), 1618–1602 (C=N), 1269 (O–CH₂). ¹H-NMR (CDCl₃) δ/ppm , 0.99 (t, 6H, CH₃), 1.06 (d, 6H, CH₃), 1.34 (m, 2H, CH₂), 1.53–1.94 (m, 24H, CH and CH₂), 4.00 (s, 6H, OCH₃), 4.02–4.24 (2t and 2dd, 12H, OCH₂), 6.97 (d, 2H, Ar), 7.02 (d, 4H, Ar), 7.28 (s, 4H, Ar), 7.31 (dd, 2H, Ar), 7.57 (d, 4H, Ar), 7.64 (2d, 6H, Ar), 8.09 (d, 4H, Ar), 8.44 (s, 2H, CH=N).

2.1.31. Synthesis of Compound 6d

Yield 56%. Elemental analysis (%): found, C 76.28, H 7.63, N 2.40; calculated (C₇₄H₈₈N₂O₁₀), C 76.26, H 7.61, N 2.40. IR (KBr) ν/cm^{-1} , 2932–2854 (C–H alkyl), 1712 (C=O ester), 1620–1603 (C=N), 1269 (O–CH₂). ¹H-NMR (CDCl₃) δ/ppm , 0.99 (t, 6H, CH₃), 1.06 (d, 6H, CH₃), 1.34 (m, 2H, CH₂), 1.52–1.92 (m, 28H, CH and CH₂), 4.00 (s, 6H, OCH₃), 4.03–4.26 (2t and 2dd, 12H, OCH₂), 6.97 (d, 2H, Ar), 7.02 (d, 4H, Ar), 7.28 (s, 4H, Ar), 7.31 (dd, 2H, Ar), 7.57 (d, 4H, Ar), 7.63 (2d, 6H, Ar), 8.09 (d, 4H, Ar), 8.44 (s, 2H, CH=N).

2.1.32. Synthesis of Compound 6e

Yield 68%. Elemental analysis (%): found, C 76.50, H 7.80, N 2.36; calculated (C₇₆H₉₂N₂O₁₀), C 76.48, H 7.77, N 2.35. IR (KBr) ν/cm^{-1} , 2931–2853 (C–H alkyl), 1711 (C=O ester), 1616–1603 (C=N), 1270 (O–CH₂). ¹H-NMR (CDCl₃) δ/ppm , 0.99 (t, 6H, CH₃), 1.06 (d, 6H, CH₃), 1.34 (m, 2H, CH₂), 1.41–1.94 (m, 32H, CH and CH₂), 4.00 (s, 6H, OCH₃), 4.01–4.24 (2t and 2dd, 12H, OCH₂), 6.96 (d, 2H, Ar), 7.02 (d, 4H, Ar), 7.28 (s, 4H, Ar), 7.32 (dd, 2H, Ar), 7.57 (d, 4H, Ar), 7.63 (s and d, 6H, Ar), 8.09 (d, 4H, Ar), 8.44 (s, 2H, CH=N).

2.1.33. Synthesis of Compound 6f

Yield 58%. Elemental analysis (%): found, C 76.71, H 7.93, N 2.30; calculated (C₇₈H₉₆N₂O₁₀), C 76.69, H 7.92, N 2.29. IR (KBr) ν/cm^{-1} ,

2930–2852 (C-H alkyl), 1715 (C=O ester), 1620–1602 (C=N), 1272 (O-CH₂). ¹H-NMR (CDCl₃) δ/ppm, 0.99 (t, 6H, CH₃), 1.06 (d, 6H, CH₃), 1.34–1.93 (m, 38H, CH and CH₂), 4.00 (s, 6H, OCH₃), 4.03–4.26 (2t and 2dd, 12H, OCH₂), 6.96 (d, 2H, Ar), 7.02 (d, 4H, Ar), 7.28 (s, 4H, Ar), 7.30 (dd, 2H, Ar), 7.57 (d, 4H, Ar), 7.63 (2d, 6H, Ar), 8.09 (d, 4H, Ar), 8.43 (s, 2H, CH=N).

2.1.34. Synthesis of Compound 6g

Yield 69%. Elemental analysis (%): found, C 76.90, H 8.09, N 2.24; calculated (C₈₀H₁₀₀N₂O₁₀), C 76.89, H 8.07, N 2.24. IR (KBr) ν /cm⁻¹, 2924–2852 (C-H alkyl), 1714 (C=O ester), 1616–1602 (C=N), 1268 (O-CH₂). ¹H-NMR (CDCl₃) δ/ppm, 0.99 (t, 6H, CH₃), 1.06 (d, 6H, CH₃), 1.34–1.93 (m, 42H, CH and CH₂), 4.00 (s, 6H, OCH₃), 4.03–4.24 (2t and 2dd, 12H, OCH₂), 6.96 (d, 2H, Ar), 7.02 (d, 4H, Ar), 7.28 (s, 4H, Ar), 7.31 (dd, 2H, Ar), 7.57 (d, 4H, Ar), 7.64 (2d, 6H, Ar), 8.09 (d, 4H, Ar), 8.44 (s, 2H, CH=N).

2.1.35. Synthesis of Compound 6h

Yield 51%. Elemental analysis (%): found, C 77.10, H 8.21, N 2.20; calculated (C₈₂H₁₀₄N₂O₁₀), C 77.08, H 8.20, N 2.19. IR (KBr) ν /cm⁻¹, 2919–2851 (C-H alkyl), 1716 (C=O ester), 1621–1603 (C=N), 1272 (O-CH₂). ¹H-NMR (CDCl₃) δ/ppm, 0.99 (t, 6H, CH₃), 1.06 (d, 6H, CH₃), 1.34–1.92 (m, 46H, CH and CH₂), 4.00 (s, 6H, OCH₃), 4.03–4.27 (2t and 2dd, 12H, OCH₂), 6.95 (d, 2H, Ar), 7.00 (d, 4H, Ar), 7.28 (s, 4H, Ar), 7.31 (dd, 2H, Ar), 7.57 (d, 4H, Ar), 7.63 (s and d, 6H, Ar), 8.09 (d, 4H, Ar), 8.43 (s, 2H, CH=N).

2.2. Characterization

All intermediates and title compounds were characterized using several spectroscopic techniques. The samples were analyzed in the form of KBr pellets and the spectra were recorded in the range of 4000–400 cm⁻¹ using a Perkin Elmer 2000 FT-IR spectrophotometer. The ¹H-NMR spectra were obtained using a Bruker 400 MHz UltrashieldTM FT-NMR spectrometer. The samples were prepared in CDCl₃ solutions with TMS as internal standard. For compounds with partial solubility in CDCl₃ at room temperature, spectrometer internal heater was used to maintain the temperature at 50°C throughout the analyses. Carbon, Hydrogen, and Nitrogen (CHN) microanalyses were performed using a Perkin Elmer 2400 LS Series CHNS/O analyzer. The liquid crystalline textures were observed using a Carl Zeiss Axioskop 40 polarizing microscope equipped with a Linkam LTS350 hotstage and TMS94 temperature controller. The heats of fusion and phase transition

temperatures of the compounds were subsequently determined with a Seiko DSC6200R differential scanning calorimeter at the heating and cooling rate of $\pm 5^\circ\text{C min}^{-1}$. The X-ray diffraction studies were performed with a Bruker D8 diffractometer (CuK_α line) equipped with a Göbel mirror, Vantec linear detector and vertical goniometer. Sample temperature was controlled by Anton Paar heating stage and the θ - θ scans were performed every 0.5°C . Prior to the measurements, the samples were heated to the isotropic phase and cooled slowly into the smectic phase to obtain the homeotropic alignment. All measurements were performed on one surface free sample. For the conformational study of the trimers, the MM2 calculations were performed using the CS Chem3D Pro software produced by CambridgeSoft Corporation. Compounds **5a**, **5c**, **5e**, **5f**, and **5g** were selected for the calculations in line with the powder X-ray diffraction analyses on similar compounds.

3. RESULTS AND DISCUSSION

3.1. Thermal Properties of Compounds **5a**–**5h**

The homologous compounds **5a**–**5h** exhibit enantiotropic mesophases. The phase transition temperatures, phase sequences, and respective transitional enthalpies are given in Table 2a. The dependence of the transition temperatures on the number of methylene units, n , in the flexible alkyl spacers for compounds **5a**–**5h** upon heating is shown in Fig. 1. The DSC trace for compound **5a** is shown in Fig. 2. All compounds exhibit the predominant enantiotropic N^* phase. In addition to this, compounds **5a**–**5h** are also smectogenic. It is apparent that all transition temperatures are strongly influenced by the length and the parity of the spacers. A strong odd–even effect for all types of phase transition temperatures is observed in this series. For the melting points, pronounced attenuation is not observed on increasing n even though the alternation is strong. For SmA-N^* transition, the trimers with odd n methylene spacers exhibit significantly lower transition temperatures in comparison with the even homologues with $n - 1$. In similar manner, strong alternation is also observed for the isotropization temperatures on increasing n . For the trimers with odd n , the isotropization temperatures are derived from the unresolved N^* -BP and BP-I transitions in the DSC thermograms. Overall, the smectogenic properties are not enhanced on increasing n . For both odd and even members, the stability of the SmC^* phase decreases on increasing n and results in monotropic SmC^* phase for compounds **5f** and **5g**. For compound **5h**, the SmC^* phase is not present. For the SmA phase, the widest temperature range (38.3°C) is recorded for compound **5b** ($n = 6$) whilst the smallest

TABLE 2a. Phase Transition Temperatures ($^{\circ}\text{C}$) and Associated Enthalpies (kJ mol^{-1}) of Compounds **5a–5h** (● = Enantiotropic Phase, ○ = Monotropic Phase; only the Highest Melting Point of Crystal is Reported; Cr = Crystal, SmX = Unidentified Smectic, SmC* = Chiral Smectic C, SmA = Smectic A, N* = Chiral Nematic, BP = Blue Phase, I = Isotropic)

Compound	Cr	SmX	SmC*	SmA	N*	BP	I
5a	● 161.7 (18.2)	○ [141.1] ^a	● 190.0 ^a	● 221.7 (0.5)	● 226.9 ^b (0.3) ^b	● 226.9 ^b (0.3) ^b	●
5b	● 192.3 (86.9)		● 225.0 ^a	● 263.3 ^a	● 266.0 (18.5)		●
5c	● 148.3 (73.2)	○ [140.9] (5.7)	● 164.6 (0.1)	● 200.0 (1.5)	● 212.0 ^b (2.0) ^b	● 212.0 ^b (2.0) ^b	●
5d	● 174.5 (69.5)		● 190.5 ^a	● 216.9 ^a	● 222.2 ^a		●
5e	● 146.7 (56.2)	○ [140.6] (8.6)	● 155.4 (0.2)	● 185.6 (1.2)	● 200.8 ^b (2.9) ^b	● 200.8 ^b (2.9) ^b	●
5f	● 174.7 (81.0)		○ [174.0] ^a	● 204.7 ^a	● 211.6 (4.9)		●
5g	● 138.1 (56.7)	○ [134.0] ^d	○ [137.8] ^d (10.0)	● 170.5 (0.4)	● 187.6 ^b (3.4) ^b	● 187.6 ^b (3.4) ^b	●
5h	● 169.7 (76.6)			● 173.9 ^a	● 194.7 (5.1)		●

^aDenotes transition temperatures determined via polarizing microscopy, undetected via DSC.

^bDenotes transition temperatures and enthalpies derived from unresolved peaks.

^cDenotes SmX = SmF* for compound **5c**.

^dDenotes SmA-SmC*-SmX transition temperatures upon cooling which are not well resolved.

[] Denotes transition temperatures in formation of monotropic SmX, SmF* or SmC*, phase.

temperature range (4.2°C) is observed for the trimer with $n = 12$ spacers (**5h**). However, the decreasing tendency in smectogenic properties with increasing n does not conform to common observation in homologous series of liquid crystals and semiflexible main chain liquid crystal polymers despite few reported exceptions [15]. One of the examples is a series of trimers with three biphenyl cores and spacers with $n = 3–12$ [2]. Contrary to the smectic phases, the overall N* temperature range increases from 5.2°C (**5a**) to 20.8°C (**5h**) on increasing n with the even members exhibiting more pronounced increase than its analogues with odd n .

3.2. Optical Properties and Smectic Phase Characterization of Compounds 5A–5H

Upon cooling the SmA phase, the SmC* texture appears as broken fans coexisting with homeotropic domains. The texture is regarded as

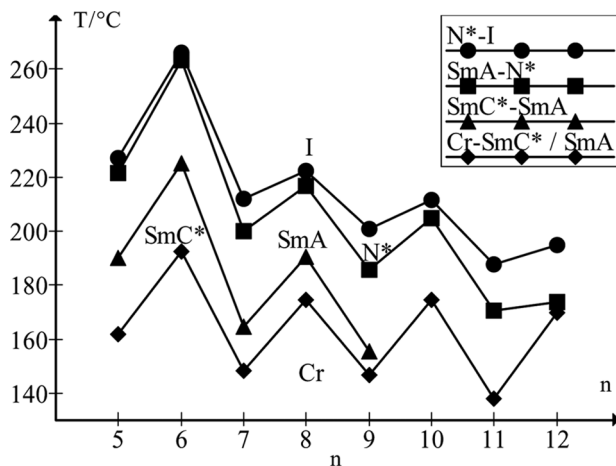


FIGURE 1 The dependence of the transition temperatures on the number of methylene units, n in the spacers for compounds **5a–5h**. The blue phase range is not depicted in this figure as it is very narrow.

pseudo-homeotropic as it is viewed along helical axis, i.e., along optic axis [16]. More distinctive dechiralization lines across the fans of the SmC* phase are observed on cooling compared to the heating run

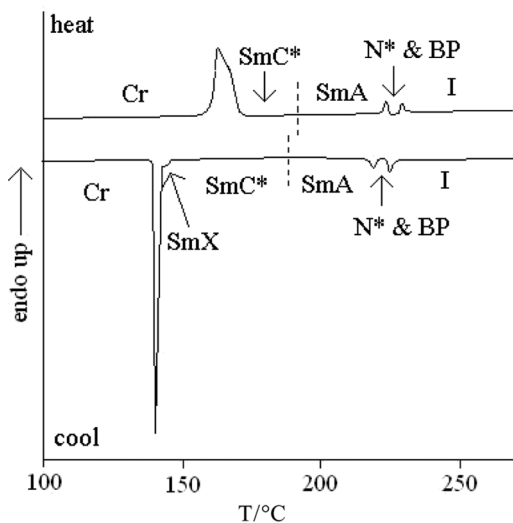


FIGURE 2 DSC trace of compound **5a** with heating and cooling rate of $\pm 5^\circ\text{C min}^{-1}$.

[17,18]. The SmA phase is assigned based on the coexistence of the fan-shaped texture and homeotropic regions [19,20]. The SmA phase is also identified by the absence of the dechiralization lines across the fans and more apparent extinct homeotropic regions. The homeotropic domains reflect the uniaxiality of the SmA phase [20]. A photomicrograph of the SmA fan-shaped texture is shown in Fig. 3.

In order to investigate the molecular organization in the smectic phases, powder X-ray diffraction is conducted for aligned sample of compounds **5a**, **5c**, **5e**, **5f**, and **5g**. For these five trimers, the plots demonstrating the layer spacing dependence upon descending temperature are given in Figs. 4a–e, respectively. The transition temperatures determined by the diffractometer is a few degrees different from the temperatures obtained via DSC. The shift in the temperatures can be due to the slight decomposition experienced by the samples which were held for several hours at high temperature before the measurements are completed.

From the powder X-ray diffraction results, for compounds **5a**, **5c**, **5e**, and **5g** exhibiting the SmA and SmC* phases, it can be observed that the transition between the orthogonal and tilted phases is of second order as indicated by the continuous decrease of layer thickness in the SmC* phase. It is, therefore, reasonable to assume that the SmA-SmC* transition for other members in this series is also second order as well. The average value of SmA layer spacing is in agreement with the MM2 approximate length of the trimer in all-*trans* conformation (i.e., for **5c**, the molecular length determined in simulation is

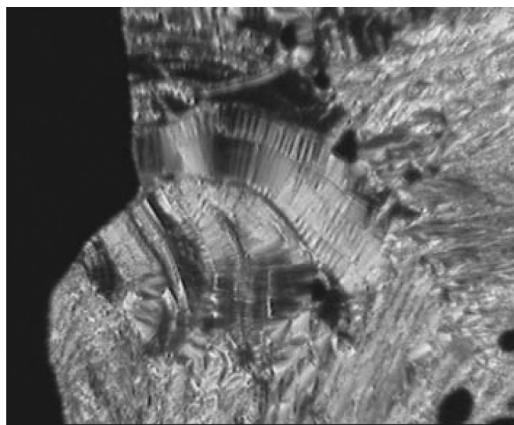


FIGURE 3 The SmA fan-shaped texture for compound **5d** at 198.2°C on heating.

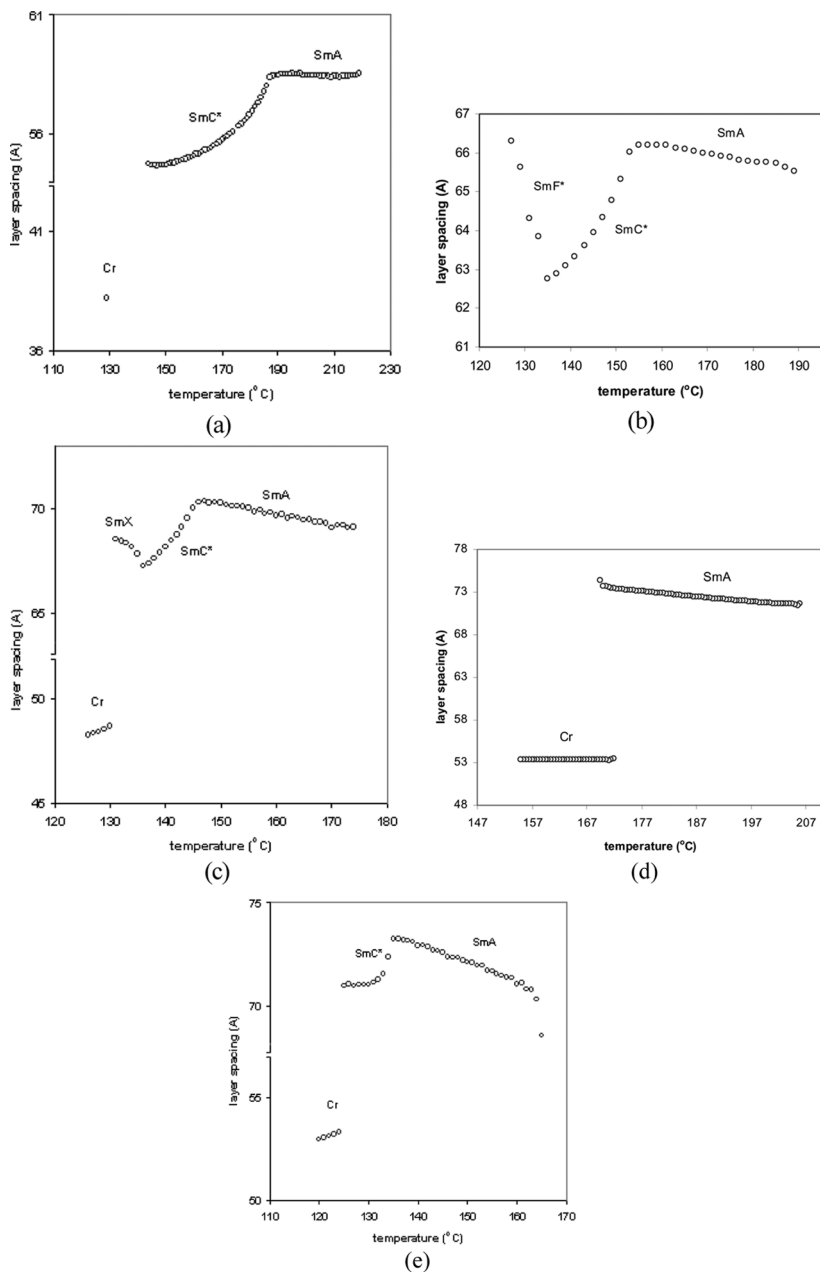


FIGURE 4 The dependence of molecular layer spacing in the smectic phases on temperature for (a) compound **5a**, (b) compound **5c**, (c) compound **5e**, (d) compound **5f**, and (e) compound **5g**.

67.5 Å, and the layer thickness is 65.9 Å), and therefore, the phase can be undoubtedly assigned as the SmA₁ (monolayer SmA) phase. At higher temperature, the slight reduction in SmA layer spacing is attributed to the tendency of the molecules from consecutive layers to intercalate and the less stretched conformation adopted by molecules preceding the N* phase. This phenomenon is not uncommon as molecules gain higher degree of fluidity and flexibility on elevating temperature. In other words, the conformational order is lower at higher temperature, and this is reflected by the decrease of layer spacing as reported in cyanobiphenyl-based dimer [4]. For the studied homologous series, the temperature influence on layer thickness is stronger upon increasing length of the alkyl spacers between the mesogenic cores. The SmA layer periodicity for compound **5g** decreases in the most apparent fashion in comparison to other odd trimers **5a**, **5c**, and **5e** in this series, indicating that the trimers with C₁₁H₂₂ spacers possess greater flexibility and fluidity to intercalate more effectively than the shorter odd counterparts. It is, therefore, suggested that long odd spacers can also be the driving force in formation of intercalated smectic phases which are usually observed for the nonsymmetric oligomers [4,19]. Upon transition to the SmC* phase, the layer periodicity decreases steadily indicating the increase in molecular tilt (to 22° for **5c** and 18° for **5e**) in the SmC* phase. As the sample is supercooled, in some homologues, the additional SmX phase is detected below the SmC* phase. Despite the increase in layer spacing in this mesophase, the periodicity remains less than the molecular length, reflecting that the molecules are tilted. From the powder X-ray diffraction analyses, the monotropic hexatic phase seems to be either the SmI* or SmF* phase. The SmI* and SmF* phases are often difficult to be distinguished from one another due to the similarities in molecular orderings between the two mesophases. However, the ambiguity in assigning the mesophase to either SmI* or SmF* can be resolved based on the textures. For compound **5c**, the hexatic phase is represented by the formation of mosaic platelets containing schlieren-like brushes (Fig. 5) upon cooling the SmC* phase. Contrary to SmI* phase which usually exhibit typical schlieren texture, the SmF* phase exhibits the mosaic-schlieren texture as reported for terephthalylidene-bis-4-n-decylaniline [16]. Thus, with the information from powder X-ray diffraction and polarizing microscopy, the monotropic hexatic phase of compound **5c** is assigned as the SmF* phase. For compound **5e**, the identification of the additional smectic phase based on the texture and powder X-ray diffraction studies is more difficult as compared to compound **5c** (Figs. 6a–c and 7).

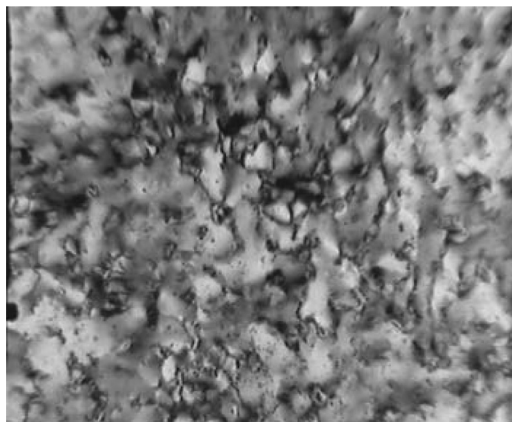


FIGURE 5 The photomicrograph of SmF mosaic-schlieren texture of compound **5c** upon cooling the SmC* phase.

3.3. The Blue Phase of Compounds **5a**, **5c**, **5e**, and **5g**

In addition to the SmC*, SmA, and N* phases, the odd trimers also exhibit the blue phase preceding the isotropic phase. With heating rate of $0.1^{\circ}\text{C min}^{-1}$, the blue phase appears slowly as the oily streaks of N* phase diminish. The blue phase is identified as BPI on the basis of its platelet texture which appears blue, red, and green in colour as shown in Fig. 8 [21]. The presence of blue phase for the trimers reflects the strong chirality of the compounds [22]. The platelet texture is more

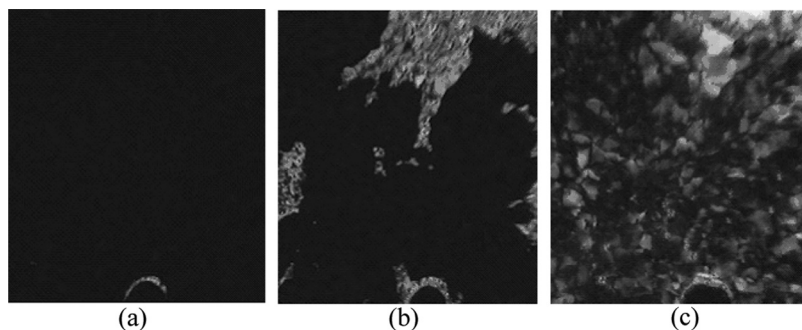


FIGURE 6 Evolution from (a) the SmA homeotropically extinct texture at 164.4°C to (b) pseudo-homeotropic texture of SmC* phase at 152.0°C to (c) the coexistence of homeotropic and platelet/fan-like texture of SmX phase at 136.0°C .

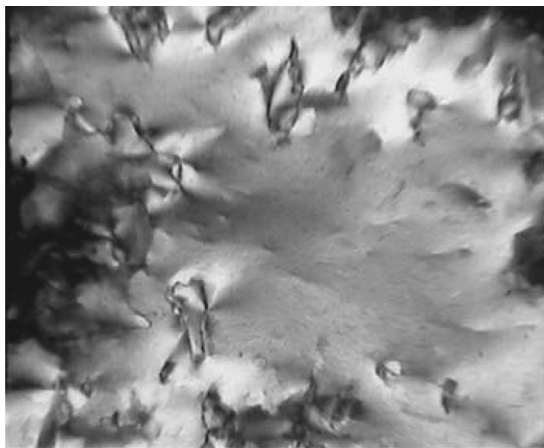


FIGURE 7 The mosaic texture of the monotropic SmX phase of compound **5e**.

apparent on cooling the isotropic phase as compared to the heating cycle. In comparison to the trimers with even spacers, the tendency for the odd members to exhibit the blue phase, whilst the even members do not, is consistent with those reported for (*R*)-2,2'-bis{6-[4-(2-(2-fluoro-4-butyloxyphenyl)pyrimidine-5-yl)phenoxy]alkoxy}-1,1'-binaphthyls and also the CBO_nO.(S)2MB dimers [7,23]. The results obtained by Blatch *et al.* [7], however, showed that there is no

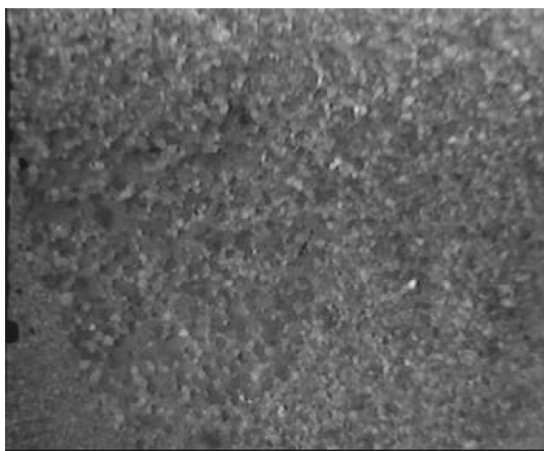


FIGURE 8 The blue phase platelet texture of compound **5e** upon cooling the isotropic phase.

apparent difference in the helical twisting power between the odd and even chiral dimers apart from a slight increase with the length of the spacer, and therefore, cannot be used to justify the presence of blue phase for the odd members.

3.4. Thermal and Optical Properties of Compounds 6a–6h

The phase transition temperatures and respective transitional enthalpies of compounds **6a–6h** are given in Table 2b. With the presence of two *meta* OCH₃ groups, pronounced differences in mesomorphic properties are observed for **6a–6h** in comparison to **5a–5h**. For **6a–6h**, the even members are nematogenic enantiotropically whilst the odd members are not mesogenic. The exclusive nematogenic behavior for even-parity trimers indicates the presence of predominant terminal intermolecular attractions rather than lateral intermolecular attractions [24]. For these compounds, a decreasing trend of N* phase temperature range is also observed with lengthening of the spacers which can be due to higher degree of flexing along the long molecular axis [24]. In other words, as the spacer length is increased, the molecules lack rigidity resulting in reduced mesomorphic properties. Although we are certain that the nematogenic characteristic for the odd trimers is absent, we are keen to investigate the possibility of these trimers exhibiting a high-order smectic phase. Hence, powder X-ray diffraction is carried out for a representative compound **6g** and the results obtained confirm the absence of smectogenic properties. The non-mesogenicity of the odd trimers can be explained by considering two

TABLE 2b. Phase Transition Temperatures (°C) and Associated Enthalpies (kJ mol⁻¹) of Compounds **6a–6h** (● = Enantiotropic Phase, ○ = Monotropic Phase, Only the Highest Melting Point of Crystal is Reported. Cr = Crystal, N* = Chiral Nematic, I = Isotropic)

Compound	Cr	N*	I
6a	● 88.8 (0.5)		●
6b	● 136.7 (50.7)	● 166.1 ^a	●
6c	● 112.7 (7.5)		●
6d	● 136.0 (60.6)	● 158.7 (3.0)	●
6e	● 110.3 (10.4)		●
6f	● 134.4 (57.7)	● 144.9 (7.6)	●
6g	● 118.0 (15.4)		●
6h	● 134.9 (75.3)	● 139.3 ^a	●

^aDenotes transition temperature determined via polarizing microscopy, undetected via DSC.

factors. Firstly, the increased molecular breadth due to *meta* OCH₃ groups hinders close intermolecular packing. Secondly, the odd-parity spacers reduce the molecular shape anisotropy with the decrease in molecular linearity. If only the first factor taken into account, only the smectogenic properties are diminished for compounds **6a–6h** owing to the lateral hindrance induced by *meta* OCH₃ groups. However, the combined effect of the two factors results in the absence of mesomorphic properties for compounds **6a**, **6c**, **6e**, and **6g**.

Our microscopic observation on compound **6b** reveals the oily streaks texture of the N* phase. Figure 9 shows the oily streaks texture in the N* matrix which possess high degree of fluidity prior to transformation into the isotropic phase [21,25]. Compound **6d**, on the other hand, exhibits the N* phase with iridescent colours of violet/blue with oily streaks present in the brightly coloured domains [26]. As shown in Fig. 10, a huge concentration of the oily streaks defects emerges gradually at the Cr-N* transition and forms a dense network throughout the microscopic sample [27]. However, the possibility of compound **6d** exhibiting BPI and BPII is ruled out as the texture does not possess the characteristics of the blue phase platelets such as the sharp edges which reflect the cubic structure of the phase [21]. At the same time, it does not contain the attributes of the amorphous texture of BPIII [28].

For the even trimers, the depression of the clearing temperatures (T_c) is largely due to the increase in molecular breadth at positions

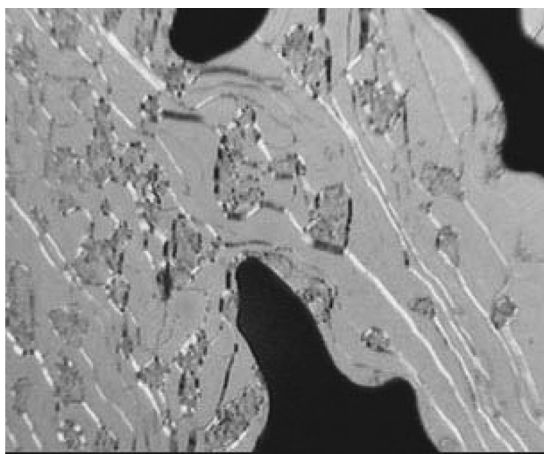


FIGURE 9 Photomicrograph of oily streaks of the N* phase during the heating cycle prior to N*-I transition (compound **6b**).

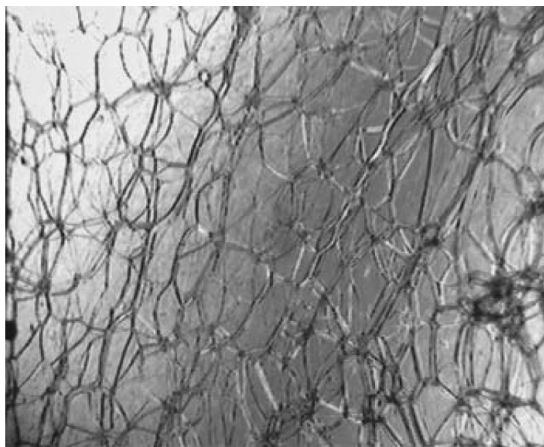


FIGURE 10 Photomicrograph of N^* phase exhibiting violet/blue iridescent colors in formation of oily streaks texture (compound **6d**).

where OCH_3 groups are introduced. The broadening of the liquid crystal molecules reduces the shape anisotropy and thus depresses the stability of the nematics [29]. It is interesting to note that the T_c for compound **5b** is 99.9°C higher than that of compound **6b** with similar spacer length. The T_c for compound **5h** is 194.7°C but upon introducing the *meta* OCH_3 groups, the T_c is reduced by 55.4°C for compound **6h** in the second series.

4. CONCLUSIONS

Every homologue in the first series of benzylidene-1,4-phenylenediamine-based liquid crystal trimers exhibited the chiral mesophases. These trimers were both smectogenic and nematogenic. The powder X-ray diffraction analyses revealed that the odd trimers also exhibited the higher-order tilted smectic phases besides the monolayer SmA and SmC* phases which was predominant in this series. For compound **5c**, the monotropic SmF* phase was identified on the basis of its mosaic-schlieren texture in support of the powder X-ray diffraction results. The odd members also exhibited the blue phase in short temperature range between the N^* and isotropic phase.

In the second series, compounds **6a–6h** with the presence of two *meta* OCH_3 groups were not smectogenic. Whilst the even trimers exhibited the N^* phase, the odd trimers were not mesogenic. The presence of lateral OCH_3 groups at the benzylidene-1,4-phenylenediamine mesogenic core suppressed the clearing temperature by nearly

100°C for compound **6b** in comparison to compound **5b** with similar spacer. For compounds **6a–6h**, the increase in molecular breadth reduced the molecular shape anisotropy and hindered lateral intermolecular interaction which is essential to induce the smectic layered arrangement. The shape anisotropy was further reduced for compounds **6a**, **6c**, **6e**, and **6g** with the presence of odd spacers resulting in the absence of mesomorphic properties.

ACKNOWLEDGMENTS

The main author (G.-Y. Yeap) acknowledges the Malaysian Higher Education Ministry and the Ministry of Science, Technology and Innovation (MOSTI) for the financial support in terms of research grants (Fundamental Research Grant Scheme, Account No. 203/PKIMIA/671025 and eScience, Account No. 305/PKIMIA/613315). The authors are also grateful to Professor Corrie T. Imrie from the University of Aberdeen, Scotland for his helpful comments and discussion regarding this work.

REFERENCES

- [1] Imrie, C. T., Stewart, D., Remy, C., Christie, D. W., Hamley, I. W., & Harding, R. (1999). *J. Mater. Chem.*, *9*, 2321.
- [2] Imrie, C. T., & Luckhurst, G. R. (1998). *J. Mater. Chem.*, *8*, 1339.
- [3] Achten, R., Koudijs, A., Karczmarzyk, Z., Marcelis, A. T. M., & Sudhölter, E. J. R. (2004). *Liq. Cryst.*, *31*, 215.
- [4] Attard, G. S., Date, R. W., Imrie, C. T., Luckhurst, G. R., Roskilly, S. J., Seddon, J. M., & Taylor, L. (1994). *Liq. Cryst.*, *16*, 529.
- [5] Mori, A., Kubo, K., Takemoto, M., & Ujiie, S. (2005). *Liq. Cryst.*, *32*, 1021.
- [6] Imrie, C. T., & Henderson, P. A. (2002). *Cur. Op. Coll. Int. Sc.*, *7*, 298.
- [7] Blatch, A. E., Fletcher, I. D., & Luckhurst, G. R. (1997). *J. Mater. Chem.*, *7*, 9.
- [8] Rokunohe, J., Yamaguchi, A., & Yoshizawa, A. (2005). *Liq. Cryst.*, *32*, 207.
- [9] Kelly, S. M., Buchecker, R., & Fünfschilling, J. (1994). *J. Mater. Chem.*, *4*, 1689.
- [10] Nishiyama, I., & Goodby, J. W. (1992). *J. Mater. Chem.*, *2*, 1015.
- [11] Meiboom, S., Sethna, J. P., Anderson, P. W., & Brinkman, W. F. (1981). *Phys. Rev. Lett.*, *46*, 1216.
- [12] Marcelis, A. T. M., Koudijs, A., & Sudhölter, E. J. R. (1999). *Mol. Cryst. Liq. Cryst.*, *330*, 1289.
- [13] Yelamaggad, C. V., Anitha Nagamani, S., Hiremath, U. S., Rao, D. S., & Prasad, S. K. (2001). *Liq. Cryst.*, *28*, 1581.
- [14] Yeap, G. Y., Hng, T. C., Mahmood, W. A. K., Adnan, R., Ito, M. M., & Youhei, Y. (2006). *Mol. Cryst. Liq. Cryst.*, *452*, 49.
- [15] Henderson, P. A., Inkster, R. T., Seddon, J. M., & Imrie, C. T. (2001). *J. Mater. Chem.*, *11*, 2722.
- [16] Gray, G. W., & Goodby, J. W. G. (1984). *Smectic Liquid Crystals—Textures and Structures*, Leonard Hill: Glasgow, UK.

- [17] Glogarova, M., Lejek, L., Pavel, J., Janovec, U., Fousek, F. (1983). *Mol. Cryst. Liq. Cryst.*, *91*, 309.
- [18] Lee, S. W., Wood, B. M., & Belcher, A. M. (2003). *Langmuir*, *19*, 1592.
- [19] Blatch, A. E., Fletcher, I. D., & Luckhurst, G. R. (1995). *Liq. Cryst.*, *18*, 801.
- [20] Queneau, Y., Gagnaire, J., West, J. J., Mackenzie, G., & Goodby, J. W. (2001). *J. Mater. Chem.*, *11*, 2839.
- [21] Singh, S. (2002). *Liquid Crystals: Fundamentals*, World Scientific Publishing Co. Pte. Ltd.: Singapore.
- [22] Pansu, B., Li, M. H., & Nguyen, H. T. (1997). *J. Phys. II Fr.*, *7*, 751.
- [23] Rokunohe, J., & Yoshizawa, A. (2005). *J. Mater. Chem.*, *15*, 275.
- [24] Cerrada, P., Marcos, M., & Serrano, J. L. (1989). *Mol. Cryst. Liq. Cryst.*, *170*, 79.
- [25] Lavrentovich, O. D., & Yang, D. K. (1998). *Phys. Rev. E.*, *57*, R6269.
- [26] Gray, G. W., & McDonnell, D. G. (1976). *Mol. Cryst. Liq. Cryst.*, *37*, 189.
- [27] Zapotocky, M., Ramos, L., Poulin, P., Lubensky, T. C., & Weitz, D. A. (1999). *Science*, *283*, 209.
- [28] Liao, G. Shashikala, I., Yelamaggad, C. V., Rao, D. S. S., Prasad, S. K., & Jáklí, A. J. (2006). *Phys. Rev. E* *73*, 051701.
- [29] Kelker, H., & Hatz, R. (1980). *Handbook of Liquid Crystals*, Verlag Chemie: Weinheim, Germany.